The Astronomical Journal, 160:241 (7pp), 2020 November https://doi.org/10.3847/1538-3881/abbd93

Spectroscopic Analysis of the Bulge Globular Cluster ESO 456-SC38*

Andrea M. Kunder and Evan Butler
Saint Martin's University, 5000 Abbey Way SE, Olympia, WA 98503, USA; akunder@stmartin.edu, embutler2015@gmail.com
Received 2020 July 29; revised 2020 September 25; accepted 2020 September 29; published 2020 November 3

Abstract

It has been suggested that the oldest stellar populations in the Milky Way are tightly bound and confined to the central regions of the Galaxy. This is one of the reasons why a handful of globular clusters located in the bulge region are thought to be remnants of the primeval formation stages of the Milky Way. The globular cluster, ESO 456-SC38 (Djorgovski 2), is one such cluster; it has a blue horizontal branch, is projected very close to the center of the Galaxy, and has an orbit confining it to the bulge/bar region. The first α abundances of seven stars in this heavily reddened cluster are presented using Apache Point Observatory Galaxy Evolution Experiment Data Release 16. A significant spread in the abundances of N, C, Na, and Al indicates the presence of multiple stellar populations in this cluster. Using Gaia DR2 proper motions and radial velocities from the Bulge Radial Velocity Assay for RR Lyrae stars, we confirm that RR Lyrae stars belong to this globular cluster.

Unified Astronomy Thesaurus concepts: Globular star clusters (656); Stellar astronomy (1583); Galactic bulge (2041); Milky Way dynamics (1051); Chemical abundances (224); Stellar abundances (1577); Stellar populations (1622)

1. Introduction

Globular clusters (GCs) have played a pivotal role in the process of deciphering the formation history of the Galaxy (e.g., Brodie & Strader 2006). These clusters are among the oldest objects in the Galaxy, and understanding their formation mechanism sheds light on both the formation timescale and conditions of the Milky Way (e.g., VandenBerg et al. 2013; Massari et al. 2019). Milky Way formation models and an understanding the globular cluster system are linked to constraints on the individual stellar components in the GCs (e.g., Muratov & Gnedin 2010; Renaud et al. 2017).

Observations of GCs toward the inner Galaxy are notoriously difficult due to high extinction and confusion with disk field stars along the line of sight (e.g., Koch et al. 2017). This has contributed to the population of GCs in the Galactic bulge being not only understudied but also incomplete (e.g., Bica et al. 2019). There has been some work focused on obtaining deep and uniform color–magnitude diagrams (CMDs) of the bulge GCs (e.g., Minniti et al. 2017; Kerber et al. 2019; Saracino et al. 2019), and recent spectroscopic surveys of GC stars have also come to the forefront (e.g., Usher et al. 2017; Vásquez et al. 2018). This has filled in some of the gaps regarding the distances, chemistry, and kinematics of the bulge clusters.

It is apparent that the bulge GC population is diverse and harbors the most metal-rich GCs in the Galaxy. Curiously, it hosts a preponderance of clusters with metallicities of [Fe/H] ~ -1.0 dex (Pérez-Villegas et al. 2020), the majority of which have a blue horizontal branch (see, e.g., Bica et al. 2016; Cohen et al. 2018). These GCs, as well as their counterpart bulge field stars (Savino et al. 2020), are likely to be some of the oldest objects in the Galaxy (Barbuy et al. 2014, 2016, 2018a). This is because the older or more metal-poor the cluster, the bluer the horizontal branch (see, e.g., Figure 11 in Dias et al. 2016). Therefore, metal-rich GCs with a blue horizontal branch can only be explained if the cluster has an ancient age.

This study focuses on the cluster ESO 456-SC38 at $(l, b) = (+2.77, -2.50)$, a poorly studied bulge GC with [Fe/H] ~ -1.0 dex and a blue horizontal branch. Upon its discovery by Holmberg et al. (1978), it was classified tentatively as an open cluster. Using improved imaging, Djorgovski (1987) noted that ESO 456-SC38 is in fact a heavily obscured GC, and this cluster is therefore also referred to as Djorgovski 2 (or Djorg 2). The first CMD of the cluster was presented by Ortolani et al. (1997) in the optical passbands. They found a distance that placed it on the near side of the Galaxy, and the cluster's red giant branch indicated it was likely metal-rich with [Fe/H] ~ -0.5. Infrared photometry of this cluster presented by Valenti et al. (2010) yielded similar results, where they found [Fe/H] $= -0.65$ dex and $(m - M)_0 = 14.23$ mag. The deepest CMD to date is based on Hubble Space Telescope (HST) photometry (Ortolani et al. 2019). ESO 456-SC38 was found to have an [Fe/H] $= -1.11$ dex with $[\alpha/\mathrm{Fe}] = +0.4$, a distance modulus placing it on the far side of the bulge with $(m - M)_0 = 14.71 \pm 0.03$ mag, and an age of 12.7 ± 0.7 Gyr.

Spectroscopic measurements of this cluster have only recently been obtained and have been based on a paucity of cluster members. From four cluster members, Dias et al. (2016) found that ESO 456-SC38 has a radial velocity of -150 ± 28 km s^{-1}, [Fe/H] $= -0.79 \pm 0.09$ dex, and [Mg/Fe] $= 0.28 \pm 0.10$ dex. From three cluster members, Vásquez et al. (2018) found the cluster has a radial velocity of -159.9 ± 0.5 km s^{-1} and a metallicity ranging from [Fe/H] ~ -0.97 to -1.09 dex, depending on the calcium triplet calibration used. Elemental abundances for stars in this cluster are largely unknown. Within the Apache Point Observatory Galaxy Evolution Experiment Data Release 16 (APOGEE DR16) dataset, we were able to isolate seven stars in ESO 456-SC38 with robust metallicities, elemental abundances, radial velocities, and Gaia DR2 proper motions. This doubles the sample of stars with spectroscopic measurements in this cluster and is the first study to shed light on a number of elemental abundances for the stars in this

* Based on observations taken by APOGEE.

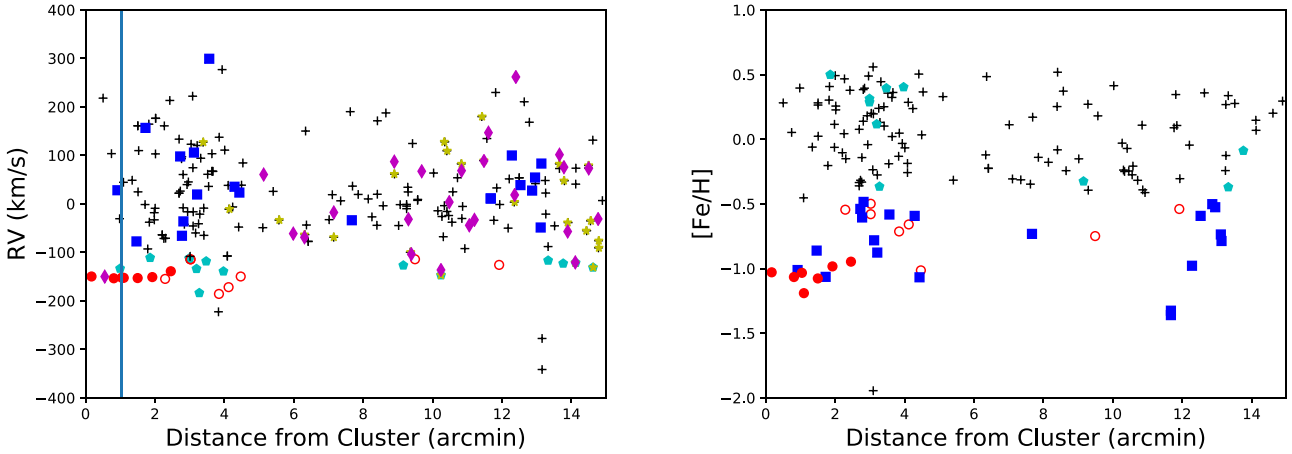

Figure 1. Left: radial distribution of radial velocities in the field around ESO 456-SC38. The vertical line at 1.′05 illustrates the half-light radius (Harris 1996, 2010 edition). Filled red circles indicate the member candidates, while open red circles indicate possible members. Cyan pentagons show stars close to the GC in radial velocity but not metallicity. Blue squares show stars close to GC in metallicity but not radial velocity. Pink diamonds show RR Lyrae stars in the BRAVA-RR dataset and gold asterisks show RR Lyrae stars from the APOGEE dataset. Error bars are the size of the points. Right: the [Fe/H] metallicities of the APOGEE stars in the field surrounding ESO 456-SC38. Member candidates are highlighted in red.

cluster. Detailed abundance analyses of stars in bulge clusters like ESO 456-SC38 are required to determine their origin—for example, whether low-latitude, metal-rich clusters formed from material that experienced a chemical enrichment history related to bulge stars—and whether multiple populations exist in these bulge clusters (e.g., Schiavon et al. 2017; Johnson et al. 2018).

2. Data and Sample

We use the most recent APOGEE data release, Sloan Digital Sky Survey-IV DR16 (Ahumada et al. 2020), to investigate the bulge globular cluster ESO 456-SC38. The APOGEE survey (Majewski et al. 2017) collects high-resolution ($R\sim$22,500) spectra of stars using near-infrared (NIR) wavelengths (Wilson et al. 2019). The spectra, in general, have a signal-to-noise (S/N) that is appropriate for elemental abundance determination ($\sim$S/N $>$ 100), and the APOGEE Stellar Parameter and Chemical Abundance Pipeline (ASPCAP; García Pérez et al. 2016) provides stellar effective temperatures, surface gravities, and metallicities precise to 2%, 0.1 dex, and 0.05 dex, respectively, for most APOGEE stars. This pipeline works especially well for red giants, which is the main population targeted by APOGEE.

APOGEE first started collecting data from bulge stars in the Northern Hemisphere, and since 2015, APOGEE-2 has begun collecting data from bulge stars in the Southern Hemisphere as well. The DR16 contains 473,307 sources with derived atmospheric parameters and abundances and is the first data release in which the newer APOGEE-2 is made public. The APOGEE DR16 catalog is ideal to search for stars in the cluster ESO-456-SC38 due to the dataset's probing of the galactic bulge in the vicinity of the cluster. We first isolated all stars in the field containing ESO-456-SC38. Cluster stars were then selected for membership using the APOGEE heliocentric radial velocity, the APOGEE [Fe/H], the projected radial distance from the center of the cluster, and Gaia DR2 proper motions.

Both the radial velocity and the [Fe/H] metallicity of ESO-456-SC38 are distinct as compared to the field stars. The radial velocity of ESO-456-SC38 is at least $\sim$50 km s^{-1} offset from the field, and the [Fe/H] metallicity is offset by at least 0.5 dex from the field (see Figure 1). Due to the scant number of stars in ESO-456-SC38 with spectroscopic measurements, it is not immediately obvious what velocity and metallicity range is compatible with cluster membership. We considered all stars within 15′ from the cluster with radial velocities within $\pm$30 km s^{-1} of the mean velocity of $-$150 km s^{-1} and within 0.5 dex of the mean [Fe/H] metallicity of $-$1.0 dex.

It is apparent that a group of seven stars is offset in both velocity and metallicity space, with velocity and metallicity values compatible with previous spectroscopic measurements for ESO-456-SC38. The velocities of these stars range from $-$139 to $-$154 km s^{-1} and the [Fe/H] metallicities range from $-$0.95 to $-$1.19 dex. The proper-motion estimate of ESO 456-SC38 reported by Vasiliev (2019) is ($\overline{\mu_\alpha}$, $\overline{\mu_\delta}$)=(0.515 $\pm$ 0.08 mas yr^{-1}, $-$3.052 $\pm$ 0.08 mas yr^{-1}) and all the cluster candidate stars we isolated have proper motions that are within 2σ of the mean proper motion of the cluster.

The tidal radius of ESO-456-SC38 is reported to be 10.′4 (from Harris 1996, 2010 edition). We adopt a limiting cluster radial distance of 15′ in an attempt to identify all APOGEE cluster members belonging to ESO-456-SC38. The group of seven stars identified above are within $\sim$3′ from the center of the cluster. We also identify two stars at a radial distance of $\sim$4.′5 with radial velocities and metallicities that may indicate they are ESO-456-SC38 cluster members. However, their proper motions are greater than 1 mas yr^{-1} offset from the mean proper motion determined for the cluster, and so we are uncertain if these stars are bona fide cluster members. As future Gaia data is released, the uncertainties on their stellar proper motions will also decrease and we can revisit the range of proper motions expected for ESO-456-SC38 cluster membership.

Figure 1 shows all APOGEE stars within 15′ from the cluster center as a function of their radial velocity and [Fe/H] metallicity. The red filled circles indicate the ESO-456-SC38 cluster candidates and the possible cluster candidates are shown with open circles. We note that the possible cluster candidates, which have [Fe/H] metallicities and radial velocities consistent with ESO-456-SC38, do not have proper motions that indicate they are moving with the cluster (see Table 1). Table 1 gives the APOGEE ID (column 1), APOGEE heliocentric radial velocity (column 2), APOGEE [Fe/H] metallicity (column 3), APOGEE [C/Fe], [N/Fe], [Na/Fe], [Mg/Fe], and [Al/Fe]

Table 1
Stellar Parameters, Elemental Abundances, Radial Velocities, and Cluster-centric Distances for Stars in ESO 456-SC38

APOGEE ID	RV (km s^{-1})	[Fe/H] (dex)	[C/Fe] (dex)	[N/Fe] (dex)	[Na/Fe] (dex)	[Mg/Fe] (dex)	[Al/Fe] (dex)	$\mu_{R.A.}$ (mas yr^{-1})	$\mu_{Decl.}$ (mas yr^{-1})	r (arcmin)	$T_{\rm eff}$ (K)	log g dex
(1)	(2)	(3)	(4)	(5)	(6)	(7)	(8)	(9)	(10)	(11)	(12)	(13)
Members												
2M18014557-2750220	−153.04 ± 0.01	−1.08 ± 0.01	−0.09 ± 0.02	0.25 ± 0.03	0.02 ± 0.07	0.34 ± 0.02	0.005 ± 0.02	0.93 ± 0.16	−3.40 ± 0.13	1.50	4157 ± 77	1.21 ± 0.07
2M18014656-2751239	−138.96 ± 0.02	−0.95 ± 0.02	−0.006 ± 0.03	0.04 ± 0.04	−0.35 ± 0.09	0.40 ± 0.02	0.18 ± 0.03	0.77 ± 0.20	−3.45 ± 0.17	2.46	4446 ± 101	1.69 ± 0.07
2M18014773-2749465	−153.48 ± 0.02	−1.07 ± 0.02	−0.07 ± 0.02	0.21 ± 0.03	−0.30 ± 0.08	0.32 ± 0.02	0.03 ± 0.03	0.39 ± 0.15	−3.27 ± 0.12	0.81	4200 ± 88	1.31 ± 0.07
2M18014786-2749080	−149.77 ± 0.01	−1.03 ± 0.01	−0.24 ± 0.02	1.03 ± 0.03	0.09 ± 0.07	0.27 ± 0.02	0.34 ± 0.02	0.52 ± 0.15	−2.95 ± 0.12	0.17	4433 ± 83	1.67 ± 0.073
2M18015130-2748086	−152.56 ± 0.01	−1.19 ± 0.02	−0.27 ± 0.02	0.29 ± 0.03	−0.12 ± 0.07	0.29 ± 0.02	−0.13 ± 0.02	0.42 ± 0.13	−3.06 ± 0.10	1.10	4066 ± 78	0.70 ± 0.07
AP18015264-2749084	−152.27 ± 0.02	−1.03 ± 0.01	−0.21 ± 0.02	0.94 ± 0.03	0.23 ± 0.07	0.27 ± 0.02	0.25 ± 0.02	0.450 ± 0.12	−2.96 ± 0.10	1.04	4438 ± 85	1.67 ± 0.07
2M18015592-2749451	−151.02 ± 0.01	−0.98 ± 0.01	−0.33 ± 0.02	1.11 ± 0.03	0.33 ± 0.07	0.27 ± 0.02	0.40 ± 0.02	0.63 ± 0.13	−3.09 ± 0.10	1.92	4423 ± 82	1.64 ± 0.07
Membership Uncertain												
2M18020645-2750472	−149.79 ± 0.02	−1.01 ± 0.01	−0.06 ± 0.02	0.26 ± 0.03	−0.10 ± 0.07	0.29 ± 0.02	0.02 ± 0.02	−2.94 ± 0.12	−5.17 ± 0.10	4.47	4361 ± 85	1.42 ± 0.07
2M18020649-2748291	−171.81 ± 0.01	−0.66 ± 0.01	0.11 ± 0.01	0.12 ± 0.02	0.09 ± 0.04	0.37 ± 0.01	0.17 ± 0.02	0.33 ± 0.11	−4.83 ± 0.09	4.12	3965 ± 70	1.07 ± 0.06
2M18011802-2742100	−144.27 ± 0.02	−0.75 ± 0.01	0.04 ± 0.02	0.04 ± 0.03	−0.17 ± 0.07	0.38 ± 0.02	0.25 ± 0.03	−6.26 ± 0.15	−6.49 ± 0.13	9.49	4305 ± 88	1.58 ± 0.06
2M18012985-2737447	−125.89 ± 0.01	−0.54 ± 0.01	0.17 ± 0.01	0.22 ± 0.01	⋯	0.34 ± 0.02	0.17 ± 0.03	−3.69 ± 0.16	−5.45 ± 0.13	11.92	3825 ± 72	0.82 ± 0.05
2M18014518-2752453	−185.77 ± 0.01	−0.71 ± 0.01	0.07 ± 0.01	0.08 ± 0.02	0.04 ± 0.06	0.35 ± 0.02	0.10 ± 0.03	−6.68 ± 0.21	−5.40 ± 0.16	3.85	4112 ± 84	1.34 ± 0.06
2M18015255-2751013	−154.78 ± 0.01	−0.55 ± 0.01	0.13 ± 0.01	0.13 ± 0.02	0.04 ± 0.06	0.33 ± 0.02	0.14 ± 0.03	−7.73 ± 0.13	−4.21 ± 0.11	2.29	4239 ± 89	1.55 ± 0.06
2M18015336-2751446	−144.70 ± 0.09	−0.58 ± 0.02	0.06 ± 0.04	0.19 ± 0.05	0.04 ± 0.11	0.67 ± 0.03	0.08 ± 0.05	−3.69 ± 0.23	0.69 ± 0.18	3.03	4836 ± 131	2.27 ± 0.05

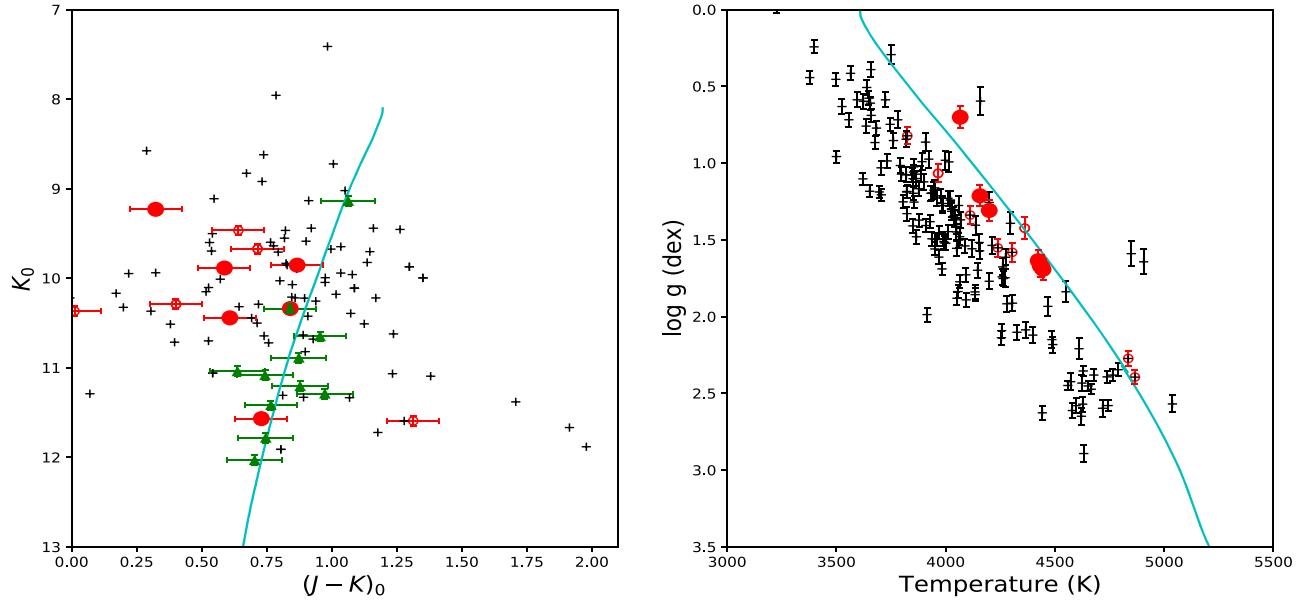

Figure 2. Left: CMD from 2MASS photometry for the stars with available APOGEE spectra and within ∼15′ of ESO 456-SC38. Member candidates are highlighted in red. Stars in the Gaia DR2 catalog located within 25″ of the cluster are shown as dark green triangles. A BaSTI isochrone of 12.5 Gyr and α-enhanced with [Fe/H] = −1.01 dex ($Z = 0.004$) (cyan line) at a distance modulus of $(m - M) = 14.71$ is also overplotted to show the approximate red giant branch of the cluster. Right: the log g vs. Teff diagram using the stellar parameters of the same APOGEE stars as in the left panel.

(columns 4–8, respectively), Gaia DR2 proper motion in R.A. and decl. (column 9 and column 10, respectively), distance from the cluster center (column 11), APOGEE effective temperature (column 12), and APOGEE surface gravity (column 13) for the ESO-456-SC38 cluster candidates and possible candidates.

Figure 2 shows the APOGEE stars with a cluster radial distance of 15′ in Two Micron All Sky Survey (2MASS) magnitude and (J − K) color dereddened using the extinctions from Gonzalez et al. (2012) and the Nishiyama et al. (2009) extinction law. From this CMD, it is apparent that these stars populate the cluster's red giant branch, although there is some scatter. We speculate the scatter arises from reddening uncertainties, due to, e.g., differential reddening within the cluster. This is because the temperatures and surface gravities, which are less sensitive to reddening uncertainties, indicate the cluster candidates are on the red giant branch of the cluster, as shown in the right panel of Figure 2 (and also see Table 1).

The BaSTI (Pietrinferni et al. 2004, 2006) α-enhanced stellar evolution models[1] were adopted to indicate the approximate location of the red giant branch of the cluster. We used the publicly available BaSTI isochrone that best matches the cluster's observed parameters, one with an age of 12.5 Gyr, a metallicity of [Fe/H] = −1.01 dex, and a distance modulus of $(m - M)_0 = 14.71$ mag. This age, metallicity, and distance modulus is consistent with previous parameters determined for the cluster (Ortolani et al. 2019). Stars from the Gaia DR2 catalog within 25′ of the cluster's center were also added for context.

3. Results

ESO 456-SC38 is one of the most confined clusters in the innermost Galaxy with an orbit that keeps it between $R_{GC} \approx$ 0.15–1.67 kpc (Pérez-Villegas et al. 2020). As discussed in the 1, this cluster is one of the curious bulge clusters belonging to the [Fe/H] ∼ −1.0 peak with a blue horizontal branch, indicating that it is very old and formed later than the bar (Ortolani et al. 2019; Pérez-Villegas et al. 2020). Further, collisionless and/or hydrodynamic simulations predict that the oldest stars reside on tightly bound orbits with small R_{GC} distances (e.g., Tumlinson 2010; Starkenburg et al. 2017). To study the primeval formation stages of the Milky Way, detailed studies of GCs such as ESO 456-SC38 are of interest.

Chemical information in the form of elemental abundance patterns is thought to be preserved in stars, and the existence of truly relic stellar groups within the Milky Way may be best uncovered using stellar abundances (e.g., Freeman & Bland-Hawthorn 2002). For example, open clusters and moving groups exhibit uniform abundance patterns (e.g., Bubar et al. 2010; Pancino et al. 2010) and old GC stars now dissolved in the Milky Way have also been uncovered from the chemical imprints (e.g., Martell & Grebel 2010; Schiavon et al. 2017). Unfortunately, very little is known about this cluster from a chemical perspective. Spectroscopic observations have been limited to seven cluster members, and the estimates of [Fe/H] for stars in this cluster range from [Fe/H] = −0.79 to −1.09 dex (Dias et al. 2016; Vásquez et al. 2018). The [Mg/Fe] measured from low-resolution (R∼2000) spectra indicates an [Mg/Fe] = 0.28± 0.10 dex for this cluster, but other than this, there have been no reports of elemental abundances of this GC.

Using the APOGEE DR16 database, we have carried out a holistic search for stars in ESO 456-SC38, looking simultaneously at radial velocity, [Fe/H], and Gaia DR2 proper motion. This has allowed the identification of cluster stars that were missed previously by GC searches in APOGEE-2 (e.g., Horta et al. 2020; Mész'aros et al. 2020). We have doubled the number of ESO 456-SC38 stars with spectroscopic measurements. From high-resolution APOGEE spectra ($R \sim$ 22,500), we find that this cluster has [Fe/H] = −1.05 ± 0.08 dex where the uncertainty represents the scatter about the mean.

[1] http://basti-iac.oa-abruzzo.inaf.it

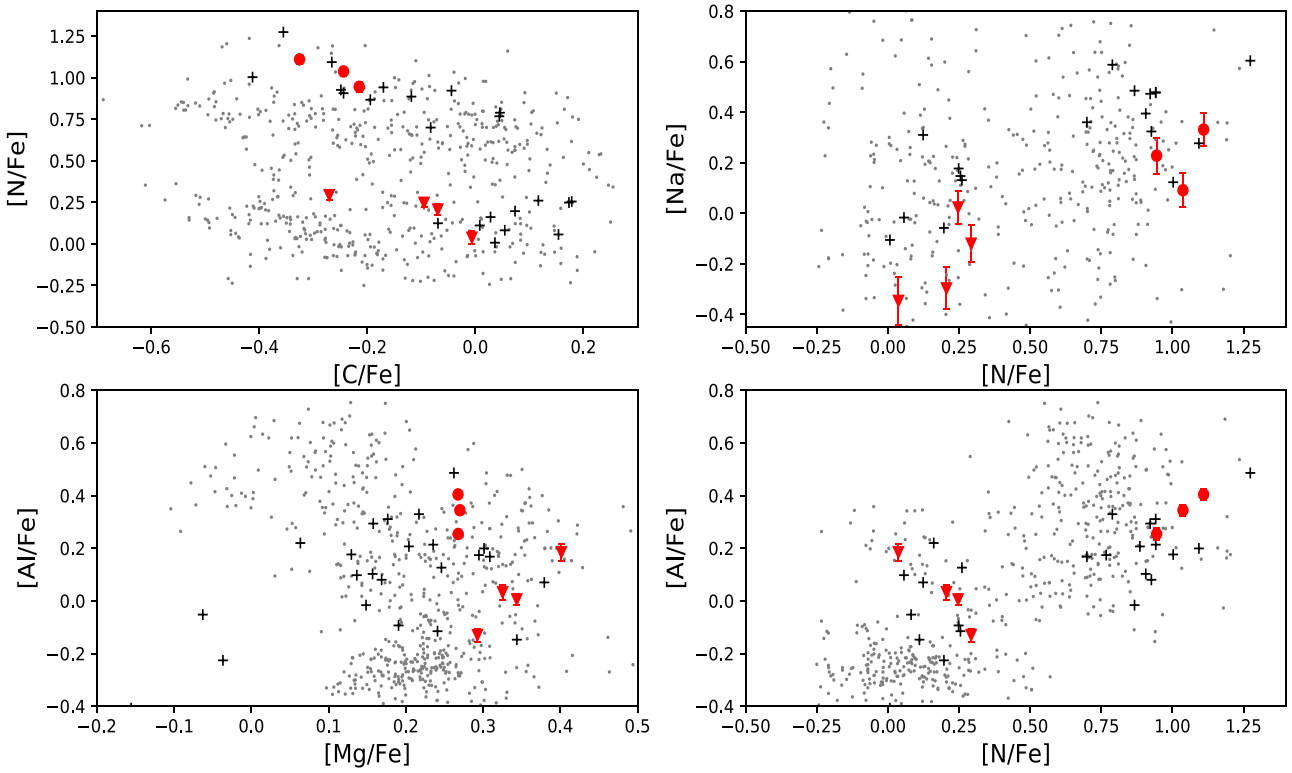

Figure 3. The abundance ratios [N/Fe], [Na/Fe], [Al/Fe], [Mg/Fe], and [C/Fe] for member ESO 456-SC38 stars highlighted in red. Filled circles represent N-enhanced stars and inverted triangles show N-normal stars. Also shown are APOGEE abundances from Schiavon et al. (2017) for stars in the inner Galaxy GCs NGC 6553, NGC 6528, NGC 6522, Terzan 5, and Palomar 6 in black and the stars from Nataf et al. (2019) in M3, M5, M107, M71, and NGC 6760 in gray.

This scatter does not seem to indicate the presence of a spread in [Fe/H] (e.g., Mész'aros et al. 2020), although our sample size is small.

We do see the clear signature of multiple populations within the cluster. Figure 3 shows the ESO 456-SC38 stars displayed in various elemental abundance planes. Multiple populations in all GCs are evident in the spread of C, N, O, and Na in cluster stars (e.g., Kraft 1994; Carretta et al. 2009), and here a bimodality is the most clearly seen within [N/Fe]. Three second-generation cluster stars are easily distinguishable in Figure 3, with [N/Fe] abundances of ∼1.0 dex and [Na/Fe] abundances of ∼0.2 dex.

Many GCs with [Fe/H] ~ -1 dex do not show a clear anticorrelation between Al and Mg abundances; instead, Mg–Al anticorrelations are typical in clusters with lower metallicities where the core temperatures of giant stars are hotter, and so where the Mg–Al cycle can operate (e.g., Shetrone 1996; Gratton et al. 2012; Mész'aros et al. 2020). All ESO 456-SC38 stars are significantly enhanced in [Mg/Fe] with a [Mg/Fe] scatter of only 0.05 dex. The N-enriched stars show [Mg/Fe] $\sim$ 0.25 dex whereas the N-normal stars have [Mg/Fe] $>\sim$ 0.3 dex. The spread in [Al/Fe] is 0.19 dex, with an uncertainty of ∼0.05 dex due to the small sample size. This is compatible to the 0.18 dex scatter reported by Mész'aros et al. (2020) for clusters with -1.3 $<$ [Fe/H] < -1.0 dex. The Al scatter could also be consistent with the slightly smaller Al scatter seen for clusters with [Fe/H] > -1.0 dex (e.g., Figure 14 of Mész'aros et al. 2020), given the small number of stars in the cluster and the uncertainties in the APOGEE elemental abundances.

Because silicon is known to be one of the most reliable α-abundance measurements in APOGEE (Jónsson et al. 2018), this element has been used as an indicator of the formation of the cluster. In particular, Horta et al. (2020) show that at metallicities of [Fe/H] ~ -1.0 dex, in situ GC subgroups have [Si/Fe] $\sim +0.25$ dex. In contrast, accreted GCs from accreted subgroups such as the Gaia-Enceladus, Helmi streams, and Sequoia have [Si/Fe] $< +0.2$ dex. We find that the average [Si/Fe] abundances of the ESO 456-SC38 stars is $\langle$[Si/Fe]$\rangle = 0.25 \pm 0.06$ dex, indicating that this cluster chemically follows the overall trend of the in situ GCs. However, to firmly categorize this cluster, information on its orbit is required (e.g., as in Pérez-Villegas et al. 2020).

3.1. RR Lyrae Stars

The horizontal branch of ESO 456-SC38 coupled with its high metallicity indicates this is an old cluster of $\sim 12.7 \pm 0.7$ Gyr (Ortolani et al. 2019). Several RR Lyrae stars (RRLs), horizontal branch stars residing on the instability strip, have been associated with this cluster. The extensive Optical Gravitational Lensing Experiment (OGLE-IV; Soszyński et al. 2019) variable star catalog lists 17 RRLs as possible members of ESO 456-SC38, and a smaller number of 7 RRLs are tabulated in the 2016 update of Clement et al. (2001). Here we attempt to ascertain RRLs that are kinematically associated with the cluster.

We crossmatch the OGLE-IV RRL stars with Gaia DR2, finding that 11 of the OGLE-IV stars associated with ESO 456-SC38 have a Gaia DR2 counterpart. Figure 4 shows proper motions of the candidate ESO 456-SC38 RRLs in proper-motion space. Most of these stars do have proper motions with values around the proper-motion estimate of ESO 456-SC38.

Using the Bulge Radial Velocity Assay for RR Lyrae stars (BRAVA-RR) dataset (Kunder et al. 2020), we verify that OGLE-BLG-RRLYR-11190 is a cluster RRL star as it has a

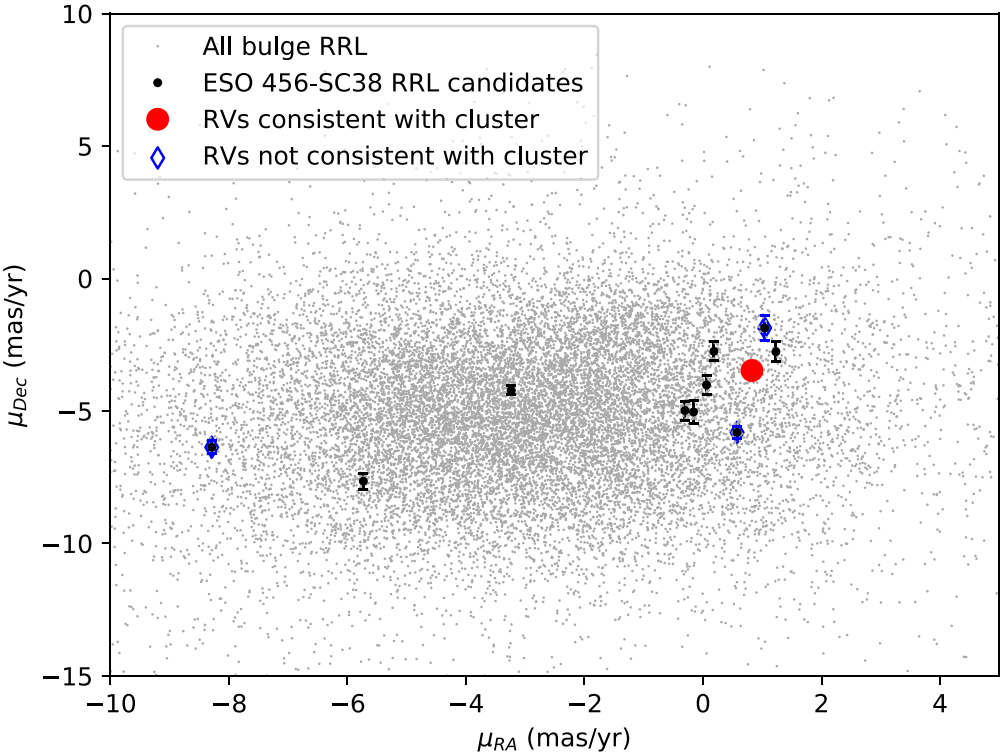

Figure 4. The Gaia DR2 proper motions of RR Lyrae stars that have been associated with ESO 456-SC38 are shown. Four of these RR Lyrae stars also have radial velocity measurements from APOGEE DR16 and/or BRAVA-RR DR2. A number of RR Lyrae stars associated with the cluster are field stars and not cluster members, but a number do have proper motions consistent with cluster membership (see Table 1).

Table 2
RR Lyrae Stars in the Vicinity of ESO 456-SC38

RRL ID	Radial Velocity (km s^{-1})	$\mu_{R.A.}$ (mas yr^{-1})	$\mu_{decl.}$ (mas yr^{-1})	r (arcmin)
(1)	(2)	(3)	(4)	(5)
Member				
OGLE-BLG-RRLYR-11190	−150 ± 5	0.83 ± 0.31	−3.47 ± 0.26	0.55
Membership Uncertain				
OGLE-BLG-RRLYR-11141	···	1.23 ± 0.46	−2.76 ± 0.37	1.84
OGLE-BLG-RRLYR-11218	···	0.18 ± 0.44	−2.75 ± 0.36	0.46
OGLE-BLG-RRLYR-11223	···	0.06 ± 0.46	−4.02 ± 0.37	0.76
Non-member				
OGLE-BLG-RRLYR-11142	60 ± 5	0.58 ± 0.30	−5.81 ± 0.22	5.13
OGLE-BLG-RRLYR-11252	127 ± 15	−8.29 ± 0.29	−6.37 ± 0.24	3.39
OGLE-BLG-RRLYR-11372	−11 ± 15	1.04 ± 0.54	−1.86 ± 0.48	4.15
OGLE-BLG-RRLYR-11049	···	−3.24 ± 0.23	−4.22 ± 0.17	4.70
OGLE-BLG-RRLYR-11060	···	−5.73 ± 0.41	−7.65 ± 0.30	3.81

radial velocity of −150 km s^{-1}. In contrast, OGLE-BLG-RRLYR-11142 has a radial velocity of 60 km s^{-1}. This RRL is not moving with the rest of the cluster and is therefore a field star instead of a cluster member.

The APOGEE dataset also includes radial velocities of a number of RRLs. Crossmatching APOGEE DR16 with OGLE-IV, we verify that OGLE-BLG-RRLYR-11190 is a cluster star with a radial velocity of −147 km s^{-1}, in good agreement with BRAVA-RR. We also find that OGLE-BLG-RRLYR-11142 with a radial velocity of 39 km s^{-1}, OGLE-BLG-RRLYR-11252 with a radial velocity of 127 km s^{-1}, and OGLE-BLG-RRLYR-11372 with a radial velocity of −11 km s^{-1} are field stars instead of cluster members. There are three RRLs with particularly similar proper motions to the mean proper motion of ESO 456-SC38, but further data, such as radial velocity values, would be helpful to confirm membership. These three RRLs are listed in Table 2 as membership uncertain RRLs.

We also notice that there are two RRLs in BRAVA-RR with radial velocities consistent with that of ESO 456-SC38, but are at a radial distance of >8′ from the cluster center (see Figure 1). These are OGLE-BLG-RRLYR-10684 and OGLE-BLG-RRLYR-11089. However, their Gaia DR2 proper motions are

considerably different that what would be expected for cluster membership.

Using the bona fide RRL cluster member, a distance to the cluster can be determined. OGLE-BLG-RRLYR-11190 has an average $V = 17.848$ mag. The absolute magnitude of the star can be found using the Gaia Collaboration et al. (2017) relation

$$M_V = 0.214\ [\mathrm{Fe/H}] + 0.88. \quad (1)$$

Adopting the mean metallicity from the red giant stars presented here of $[\mathrm{Fe/H}] = -1.05$, this gives $M_V = 0.66$ mag. An identical absolute magnitude is found using the theoretical relations from Catelan et al. (2004):

$$M_V = -2.288 - 0.882 \log(\mathrm{Z}) + 0.108 \log(\mathrm{Z})^2 \quad (2)$$

where

$$\log(\mathrm{Z}) = [\mathrm{Fe/H}] - 1.765. \quad (3)$$

Our uncertainty in M_V is ~0.03 dex, based on our uncertainty in [Fe/H]. Assuming total-to-selective absorption $RV = 3.1$, and $E(B-V) = 0.81$, the distance modulus from OGLE-BLG-RRLYR-11190 is $(m-M)_0 = 14.68 \pm 0.07$ (distance of 8.63 ± 0.28 kpc). This distance value is smaller than the distance of 9.12 kpc obtained by Ortolani et al. (2019) using RR Lyrae stars, and instead agrees very well with the distance value of 8.75 kpc obtained from CMD fitting by Ortolani et al. (2019). The distance is larger than the 6.3 kpc value in the Harris (1996) catalog which has recently been adopted for dynamical calculations in Baumgardt et al. (2019).

4. Conclusions

We present seven red giant stars from APOGEE DR16 that are members of the bulge globular cluster ESO 456-SC38. This doubles the sample of stars with spectroscopic measurements for this cluster and also adds to the number of stars associated with GCs in the APOGEE footprint (Horta et al. 2020; Mész'aros et al. 2020). From their [C/Fe], [N/Fe], [Na/Fe], [Mg/Fe], and [Al/Fe] abundances, we detect the presence of multiple stellar populations in this cluster. The average [Si/Fe] abundances of these stars is $\langle[\mathrm{Si/Fe}]\rangle = 0.25 \pm 0.06$ dex, which is typical for in situ bulge clusters (e.g., Horta et al. 2020) and in agreement with the recent orbit for this cluster from Pérez-Villegas et al. (2020). Using both radial velocities and Gaia DR2 proper motions, we show that some RRL that have been associated with the cluster are instead field stars. However, we do confirm the kinematic association of one RRL and the possible association of three more RRLs, as expected from its blue horizontal branch.

X.X.X. acknowledges support from grant AST-2009836 from the National Science Foundation. We thank the anonymous referee for suggestions that helped the clarity and quality of the paper.

ORCID iDs

Andrea M. Kunder https://orcid.org/0000-0002-2808-1370
Evan Butler https://orcid.org/0000-0002-1533-6004

References

Ahumada, R., Allende Prieto, C., Almeida, A., et al. 2020, ApJS, 249, 3
Barbuy, B., Cantelli, E., Vemado, A., et al. 2016, A&A, 591, A53
Barbuy, B., Chiappini, C., Cantelli, E., et al. 2014, A&A, 570, A76
Barbuy, B., Chiappini, C., & Gerhard, O. 2018a, ARA&A, 56, 223
Baumgardt, H., Hilker, M., Sollima, A., & Bellini, A. 2019, MNRAS, 482, 5138
Bica, E., Barbuy, B., & Ortolani, S. 2016, PASA, 33, 28
Bica, E., Pavani, D. B., Bonatto, C. J., & Lima, E. F. 2019, AJ, 157, 12
Brodie, J. P., & Strader, J. 2006, ARA&A, 44, 193
Bubar, E. J., & King, J. R. 2010, AJ, 140, 293
Carretta, E., Bragaglia, A., Gratton, R. G., et al. 2009, A&A, 505, 117
Catelan, M., Pritzl, B. J., & Smith, H. A. 2004, ApJS, 154, 633
Clement, C. M., Muzzin, A., Dufton, Q., et al. 2001, AJ, 121, 2587
Cohen, R. E., Mauro, F., Alonso-Garcia, J., et al. 2018, AJ, 156, 41
Dias, B., Barbuy, B., Saviane, I., et al. 2016, A&A, 590, 9
Djorgovski, S. 1987, ApJ, 317, L13
Freeman, K., & Bland-Hawthorn, J. 2002, ARA&A, 40, 487
Gaia Collaboration, Clementini, G., Eyer, L., et al. 2017, A&A, 605, A79
García Pérez, A. E., Allende Prieto, C., Holtzman, J. A., et al. 2016, AJ, 151, 144
Gonzalez, O. A., Rejkuba, M., Zoccali, M., et al. 2012, A&A, 543, 13
Gratton, R. G., Villanova, S., Lucatello, S., et al. 2012, A&A, 544, 12
Harris, W. E. 1996, AJ, 112, 1487
Holmberg, E. B., Lauberts, A., Schuster, H.-E., & West, R. M. 1978, A&AS, 34, 285
Horta, D., Schiavon, R. P., Mackereth, J. T., et al. 2020, MNRAS, 493, 3363
Johnson, C. I., Rich, R. M., Caldwell, N., et al. 2018, AJ, 155, 71
Jónsson, H., Allende Prieto, C., Holtzman, J. A., et al. 2018, AJ, 156, 126
Kerber, L. O., Libralato, M., Souza, S. O., et al. 2019, MNRAS, 484, 5530
Koch, A., Kunder, A., & Wojno, J. 2017, A&A, 605, 128
Kraft, R. P. 1994, PASP, 106, 553
Kunder, A., Pérez-Villegas, A., Rich, R. M., et al. 2020, AJ, 159, 270
Majewski, S. R., Schiavon, R. P., Frinchaboy, P. M., et al. 2017, AJ, 154, 94
Martell, S. L., & Grebel, E. K. 2010, A&A, 518, A14
Massari, D., Koppelman, H. H., & Helmi, A. 2019, A&A, 630, 4
Mész'aros, S., Masseron, T., & García-Hernández, D. A. 2020, MNRAS, 492, 1641
Minniti, Geisler, & Alonso-García 2017, ApJL, 849, L24
Muratov, A. L., & Gnedin, O. Y. 2010, AJ, 718, 1266
Nataf, D. M., Wyse, R. F. G., Schiavon, R. P., et al. 2019, AJ, 158, 14
Nishiyama, S., Tamura, M., Hatano, H. l., et al. 2009, ApJ, 696, 1407
Ortolani, S., Bica, E., & Barbuy, B. 1997, A&AS, 126, 319
Ortolani, S., Held, E. V., Nardiello, D., et al. 2019, A&A, 627, 145
Pancino, E., Carrera, R., Rossetti, E., et al. 2010, A&A, 511, 56
Pérez-Villegas, A., Barbuy, B., Kerber, L. O., et al. 2020, MNRAS, 491, 3251
Pietrinferni, A., Cassisi, S., Salaris, M., & Castelli, F. 2004, ApJ, 612, 167
Pietrinferni, A., Cassisi, S., Salaris, M., & Castelli, F. 2006, ApJ, 642, 797
Renaud, F., Agertz, O., & Gieles, M. 2017, MNRAS, 465, 3622
Saracino, S., Dalessandro, E., Ferraro, F. R., et al. 2019, ApJ, 874, 86
Savino, A., Koch, A., Prudil, Z., Kunder, A., & Smolec, R. 2020, A&A, 641, A96
Schiavon, R. P., Zamora, O., Carrera, R., et al. 2017, MNRAS, 465, 501
Shetrone, M. D. 1996, AJ, 112, 1517
Soszyński, I., Udalski, A., Wrona, M., et al. 2019, AcA, 69, 321
Starkenburg, E., Oman, K. A., Navarro, J. F., et al. 2017, MNRAS, 465, 2212
Tumlinson, J. 2010, ApJ, 708, 1398
Usher, C., Pastorello, N., Bellstedt, S., et al. 2017, MNRAS, 468, 3828
Valenti, E., Ferraro, F. R., & Origlia, L. 2010, MNRAS, 402, 1729
VandenBerg, D. A., Brogaard, K., Leaman, R., & Casagrande, L. 2013, ApJ, 775, 134
Vasiliev, E. 2019, MNRAS, 484, 2832
Vásquez, S., Saviane, I., Held, E. V., et al. 2018, A&A, 619, A13
Wilson, J. C., Hearty, F. R., Skrutskie, M. F., et al. 2019, PASP, 131, 055001